Influence of Pile and Soil Parameters on the Seismic Performance of RC Bridge Piers: From Global Fragility to Local Damage

Begum E. Ajom[a,*], **Kaustubh Dasgupta**[b,c], **and Arindam Dey**[b,c]

[a]Department of Civil Engineering, Indian Institute of Technology Guwahati, Assam, 781039, India
[b]Department of Civil Engineering, Indian Institute of Technology Guwahati, Assam, 781039, India
[c]Associated Faculty, Centre for Disaster Management and Research, Indian Institute of Technology Guwahati, Assam, 781039, India

*Corresponding author email address: begum176104101@iitg.ac.in (B.E. Ajom).

Abstract: Reinforced Concrete (RC) bridge piers supported on pile foundations are key structural components that must maintain resilience during seismic events. While existing studies have explored seismic fragility analyses for bridges, incorporating Soil-Structure Interaction (SSI) and hazard-related uncertainties, the specific parametric influences of piles and soil on the probability of damage in bridge piers remain largely unexplored. This study investigates the seismic behaviour of RC bridge pier-pile systems embedded in sandy soils through detailed finite element analyses that incorporate pier-pile-soil interaction using a Beam on Nonlinear Winkler Foundation (BNWF) modelling approach in OpenSees. The research systematically evaluates the influence of pile diameter, longitudinal reinforcement ratios, and soil types on both global damage probability and localized inelastic responses. Fragility analyses are performed using Incremental Dynamic Analysis (IDA) with site-specific ground motions, while strain-based limit states are used to define capacity and monitor local damage mechanisms. The extent of plastic hinge formation in both pier and pile components is used to assess section-level deformation demands. The results indicate that piles designed as per current Indian Standards tend to show linear-elastic behaviour during low to moderate level earthquake shaking, thereby concentrating the seismic damage in the piers which are easier to inspect and retrofit. However, reduction in pile diameter or provision of low longitudinal reinforcement ratio in the pile, leads to inelastic behaviour of the piles. Thus, the overall inelastic behaviour of the pier-pile-soil system gets distributed among the pier and the piles. The findings highlight the importance of pile and soil parameters for the desirable seismic performance of both pier and the piles while ensuring ease of post-earthquake repair. A novel curvature-based approach is also proposed to estimate plastic hinge length in pile-supported piers, contributing valuable insights for the seismic assessment and design of RC bridge foundations in earthquake-prone regions.

Keywords: Bridge piers; Pile foundations; Soil-structure interaction; Fragility curves; Local damage; Plastic hinge zones.

1. Introduction

Seismic vulnerability of Reinforced Concrete (RC) bridge pier-pile foundation systems is significantly influenced by structural and geotechnical parameters. These factors affect the interaction between the soil, pile, and structure, which in turn impacts the seismic performance of the bridge piers. While many researchers have conducted seismic fragility analyses for the risk assessment of bridges at both system and component levels considering Soil-Structure Interaction (SSI) [1,2], fragility curves have also been utilized as a tool for comparative studies to evaluate the influence of various modelling approaches and parametric variations on seismic performance of bridges. For instance, the impact of different SSI modelling methods on the seismic fragility curves was studied for a common bridge configuration found in central and eastern USA [3].

Several studies have specifically evaluated the fragility of bridge pile-group foundations, particularly in the context of scouring action during flood scenarios [4], soil liquefaction, and seismic actions. The time-dependent effects of scour progression due to future flood events have been analysed using fragility curves under seismic loading, highlighting the increasing vulnerability of bridges over their service life [4]. The sensitivity of fourteen structural and soil parameters on the seismic performance of pier-pile-group in liquefiable ground was evaluated by using fragility curves [5]. Seismic fragility functions for reinforced concrete bridges under both earthquake-only and earthquake-plus-scouring conditions were also studied in detail [6]. More recently, the structural fragility of pile foundations subjected to flood-related scenarios was determined by considering the contribution of bridge scour and hydrodynamic load [7].

Additionally, fragility analyses have been conducted to investigate the effects of ground motion parameters on the seismic response of pile-supported structures. The directional uncertainties of earthquake-induced ground motions were evaluated on pile-supported wharves, identifying high-damage zones through fragility surfaces [8]. The seismic fragility of pile-supported structures was obtained under mainshock-aftershock sequences and it was found that aftershocks significantly increase damage probabilities compared to mainshock-only scenarios [9]. While these studies provide valuable insights into hazard-related uncertainties and ground motion influences on bridge systems, the effects of structural and geotechnical properties of the foundation on the seismic behaviour of RC bridge piers remain largely unexplored.

Recent studies by [10,11] examined soil-monopile-pier systems through nonlinear static and incremental dynamic analyses, respectively. Their studies investigated the effects of axial load, pile diameter, and soil properties on seismic fragility, noting that increased pile diameter and axial loads improved system performance. However, a comprehensive understanding of the seismic behaviour of pile-group-supported piers, particularly the parametric influence of pile and soil properties on bridge piers, is still lacking. This gap can be addressed through fragility analyses to evaluate pier response at a global level.

Case histories from past earthquakes indicate that, in addition to pier yielding, pile shafts inevitably undergo nonlinear deformation during strong seismic events. At the local level, the behaviour of piers and piles can be examined by assessing their ductile responses, particularly by observing the formation and evolution of nonlinear plastic hinge zones. Several researchers have investigated the plastic hinge length and location in single pile shafts, considering various factors such as soil conditions, pile properties, seismic design levels, and liquefaction effects [12-15]. Recently, the ductile behaviour of pile-group foundations has been studied by [16,17]. These researchers conducted detailed parametric studies to identify critical structural and soil parameters affecting the seismic performance of scoured pile-group foundations. Their studies concluded that pile-group foundations possess considerable ductility and strength capacity. Furthermore, they proposed limit states for scoured pile groups based on the development of plastic hinges in the pile shafts. The existing studies have primarily investigated plastic hinge formation in single pile shafts and pile-group foundations but have not comprehensively addressed the issues with plastic hinge formation in a pier-pile-soil integrated system. A critical gap remains in understanding how yielding in piles influences the seismic performance of piers, particularly in redistributing demands and mitigating excessive curvature ductility in pier sections. Additionally, a systematic evaluation of the effects of varying pile and soil parameters on the plastic hinge development on both pier and piles are not well quantified.

The present study evaluates the damage probability of an RC bridge pier in sandy soil by incorporating the parametric influences of pile and soil properties through a detailed pier-pile-soil interaction analysis. The seismic behaviour of the overall pier-pile-soil system is assessed through fragility analyses, wherein the influence of the pile and soil on the seismic vulnerability of the piers is studied. Subsequently, the extent of section level damage is investigated by observing the formation of plastic hinges in both pier and the piles. Specifically, pile diameter, longitudinal reinforcement ratio in piles and the soil properties are varied for the pier-pile-soil system, as these factors are expected to significantly affect the seismic response of the pier-pile system. The novelty of the present study lies in the investigation of how the pile and soil parameters can influence the vulnerability of the pier during earthquake shaking. The findings of this study aim to enhance the understanding for improving the design and assessment of pile-supported bridge piers in earthquake-prone regions.

2. Finite-element modelling

In the present study, numerical analyses are conducted in the open-source software platform OpenSees [18] to evaluate the seismic response of RC bridge piers considering pile-soil interaction. To accurately capture the complex behaviour of the pier-pile-group foundation system, nonlinearity has been introduced in both soil and structural components by assigning appropriate constitutive material models, as detailed in the subsequent subsections.

2.1. Modelling of piles and pier

The RC pier and piles are modelled using Displacement-Based beam-column Elements (DBEs) with fibre sections to accurately capture material nonlinearity and the interaction between axial force and bending moment. The cross-sections of the RC members are discretized into fibres consisting of cover concrete, core concrete and longitudinal steel reinforcement as illustrated in Fig. 1(a). The efficacy of fibre-based models in enabling spread of plasticity and material nonlinearity across the cross-section and length of a member is critical for accurately capturing the progression of localized damage at any point in the structural member.

The concrete fibres, both core and cover, are modelled using *Concrete02* material model, which incorporates linear tension softening of concrete (Fig. 1(b)). The properties of confined and unconfined concrete are determined based on the relationships proposed by [19, 20]. The axial stress-strain behaviour of the reinforcing steel is simulated using the *Steel02* material model (Fig. 1(c)) which corresponds to the Giuffre-Menegotto-Pinto model with kinematic and isotropic strain hardening [21, 22].

Mesh sensitivity analyses conducted separately under both static and dynamic loading conditions indicate that an element length of 0.5 m provides satisfactory accuracy for both global and local responses. Therefore, this element length is consistently used for modelling both the pier and the piles throughout the study.

2.2. Modelling of soil-pile interaction

The dynamic SSI analysis in this study is performed using the Beam on Nonlinear Winkler Foundation (BNWF) technique, which involves two sequential steps. Firstly, a nonlinear site response analysis is carried out to determine the free-field motions within the soil deposit. Secondly, the pile-soil interaction is evaluated using a BNWF model where the pile is connected to a series of nonlinear soil springs and the free-field displacement time histories (DTHs) at each depth obtained from the site response analysis are applied to the soil-end nodes of the lateral springs as an excitation to the system.

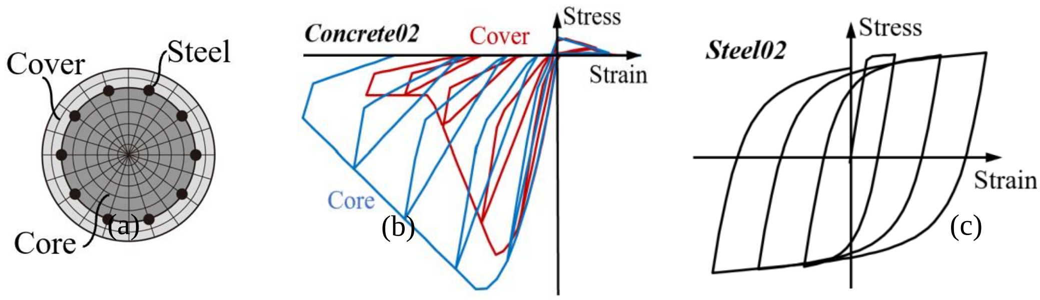

Fig. 1. Numerical modelling of structural member: (a) fibre section discretisation of pier and piles; (b) concrete model; (c) steel model.

2.2.1 Site response analysis

One-dimensional nonlinear site response analysis is performed using OpenSees, assuming horizontally layered soil deposits underlain by a uniform half-space and subjected to vertically propagating shear waves. The soil is modelled in two dimensions as a soil column using the plane strain formulation of quadrilateral elements (Fig. 2(a)), where each node has two translational Degrees of Freedom (DoFs). The nodes sharing same elevations are tied to one another in both the translational DoFs in order to achieve a simple shear deformation pattern. To simulate the nonlinear hysteretic behaviour of sandy soils, the Pressure-Dependent Multi-Yield (PDMY) material model (Fig. 2(b)) is employed. This advanced constitutive material model captures the stress-dependent behaviour of sandy soils and effectively accounts for the increase in confining pressure on the pile with increasing embedment length of pile. A general schematic of the model is shown in Fig. 2(c).

2.2.2 Methodology for BNWF approach

Soil in the BNWF model is represented through a series of discrete nonlinear macro-elements that consists of springs and dashpots. For the lateral soil-pile interaction, the nonlinear behaviour is characterized as consisting of visco-elastic, plastic and gap components in series [23]. The visco-elastic element consists of an elastic spring and a damper in parallel to simulate radiation damping in the system. The plastic component is simulated by developing a relationship between the lateral pile deflection, y, and the soil resistance, p, known as the $p-y$ curve. Similarly, the nonlinear behaviour of the axial resistance of the pile along the pile shaft and the end bearing resistance at the pile tip is modelled using the visco-elastic and plastic components in series. $t-z$ and $Q-z$ curves are then used to simulate the plastic components of the respective macro-elements. These macro-elements, often referred to as soil springs, are implemented using zero-length elements. Each zero-length element connects two nodes: the pile end node and the soil end node, both located at the same spatial position. A schematic of the dynamic BNWF model is presented in Fig. 3(a). The macro-elements are assigned with the uniaxial material objects *PySimple1*, *TzSimple1* and *QzSimple1*, available in OpenSees, to model the lateral and axial springs, respectively. The generic cyclic behaviours of these material models are depicted in Figs. 3(b), 3(c) and 3(d), where F represents the soil resistance and Δ denotes pile deflection.

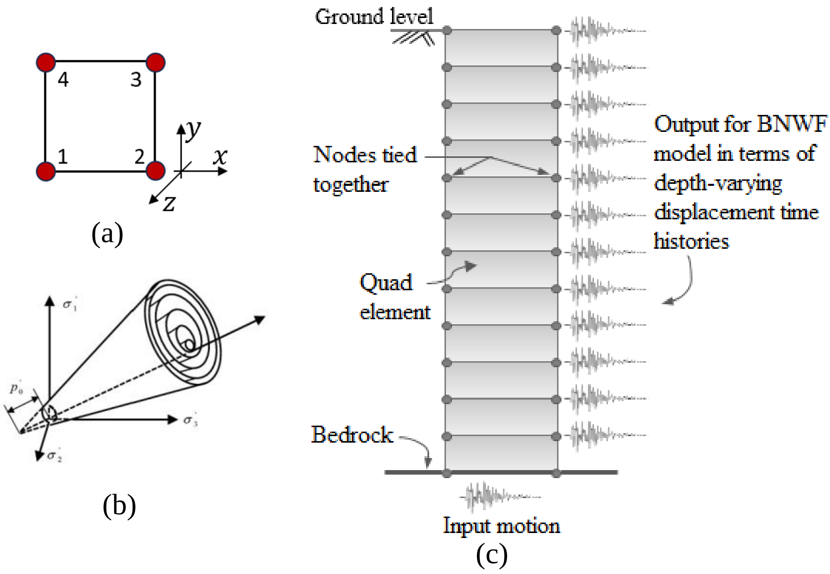

Fig. 2. (a) Plane strain quadrilateral element; (b) Yield surface configuration of pressure dependent soil material model [24]; (c) Schematic representation of a soil column for site-response analysis.

In this study, the soil springs are characterized based on the recommendations provided in [25] guidelines. The key input parameters required by the *PySimple1* material to construct the backbone of the $p - y$ curves, which approximates the API sand relationship, include the ultimate soil resistance, p_u and the displacement y_{50}, at which 50% of the ultimate soil resistance is mobilised under monotonic loading. These parameters are calculated using the equations provided by [26], as adopted in the API standards.

The ultimate shaft frictional resistance, t_u (kN/m) mobilized along the embedded length of the pile in sandy soil is calculated using the equation proposed by [27]. The corresponding z_{50} values are calculated based on a $t - z$ curve recommended by [28]. The end bearing capacity of the pile tip is computed using the relation proposed by [29] and the corresponding z_{50} value is calculated based on the $Q - z$ curve proposed by [30].

Previous studies have shown that radiation damping is negligible as compared to material damping in the vicinity of a pile when the soil exhibits pronounced hysteretic behaviour with significant plastic deformations [31]. As a result, radiation damping is not considered in this study.

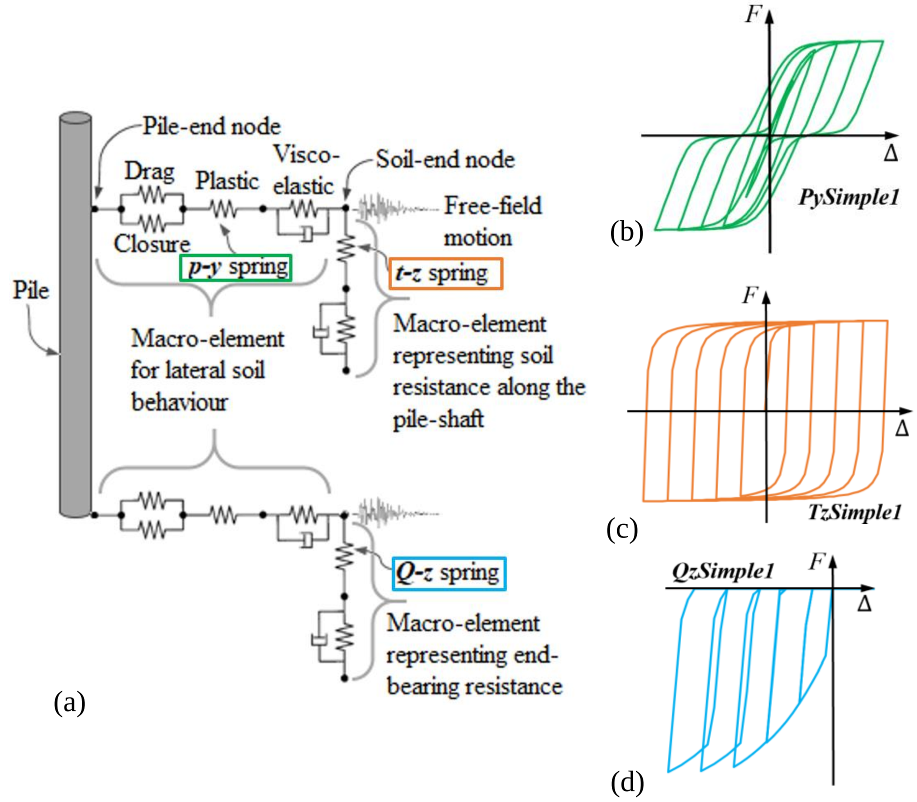

Fig. 3. BNWF modelling: (a) schematic illustration of the spring-dashpot-pile model; (b) $p-y$ spring; (c) $t-z$ spring; and (d) $Q-z$ spring.

3. Numerical model validation

Validation of the numerical model is an essential step to establish its reliability and sufficiency before performing detailed analyses. In this study, two validation exercises have been carried out. The first validation focuses on a fixed-base pier, evaluating the nonlinear behaviour of structural members to affirm the suitability of the material models and finite-elements used. The second validation examines the BNWF approach to confirm its effectiveness in capturing SSI effects under seismic loading.

3.1. Validation of nonlinear behaviour of structural member

An RC hollow rectangular bridge pier, as illustrated in Fig. 4(a), has been modelled with fibre sections, and a nonlinear static analysis is carried out in OpenSees. The model is validated by reproducing the cyclic test results of a 5.6 m pier from the tested bridge model B213C, as obtained from the experiments conducted by [32]. Further details, including reinforcement specifications, can be found in the studies by [32, 33].

As shown in Fig. 4(b), the force-displacement response at the pier head, derived from the numerical analysis is compared with the experimental result. The numerical model effectively captures the cyclic response of the pier up to the onset of strength degradation. The backbone curve of the Giuffre-Menegotto-Pinto model follows a bilinear form with isotropic strain-hardening characteristics; therefore, the steel material model used in this study does not account for cyclic strength and stiffness degradation due to bar buckling and fatigue [34]. Capturing these phenomena would require alternative modelling approaches with different steel material models. However, since this research does not focus on the pier response beyond the onset of strength degradation, these aspects are not considered in this study.

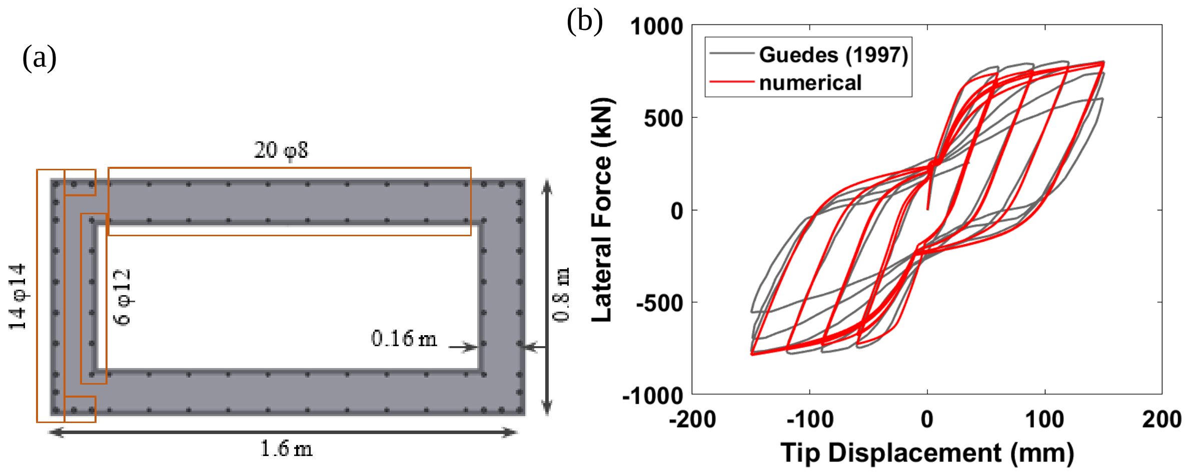

Fig. 4. (a) Cross-sectional details; and (b) Force-displacement response of the RC rectangular hollow pier.

3.2. Validation of dynamic BNWF approach

The validity of the dynamic BNWF approach in predicting the seismic response of a pile-soil system is evaluated by numerically simulating the behaviour of a single steel pile under a centrifuge test (No. 12) conducted in a previous study [35]. The steel pile is embedded in a homogeneous sandy soil profile as shown in Fig. 5. A horizontal acceleration record (Fig. 6) with a peak acceleration of 0.15 g is given as the input at the base of the system.

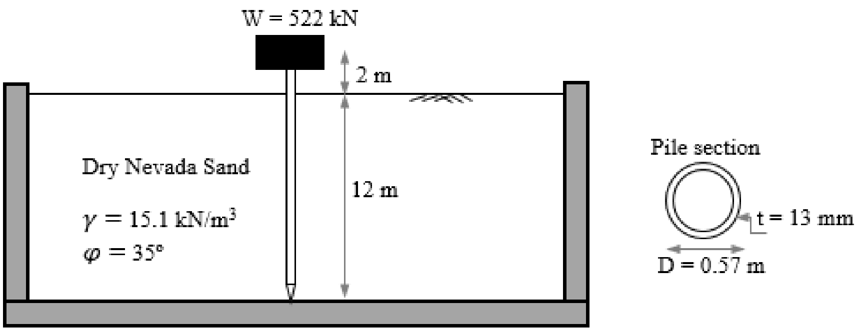

Fig. 5. Prototype model of the single pile centrifuge test [35].

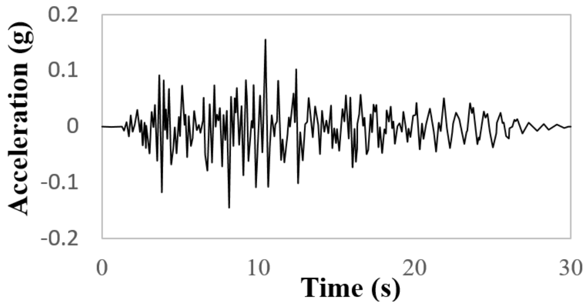

Fig. 6. Input acceleration time history for the centrifuge test [35].

Fig. 7(a) compares the spectral acceleration of the free-field motions at the ground surface obtained from the numerical site response analysis with that of the centrifuge test. A good agreement is observed between the experimental and numerical results.

Fig. 7(b) presents the acceleration response spectra of the pile-head motion, comparing the numerical result of the BNWF model with the centrifuge test data. The numerical simulation exhibits a slightly stiffer response, with the spectral peak occurring at 0.9 sec., whereas the experimental data shows the peak at 1 sec. Additionally, the peak spectral acceleration of the pile head is slightly overestimated in the numerical model. Nevertheless, the overall agreement between numerical and experimental results is satisfactory for both soil and pile responses.

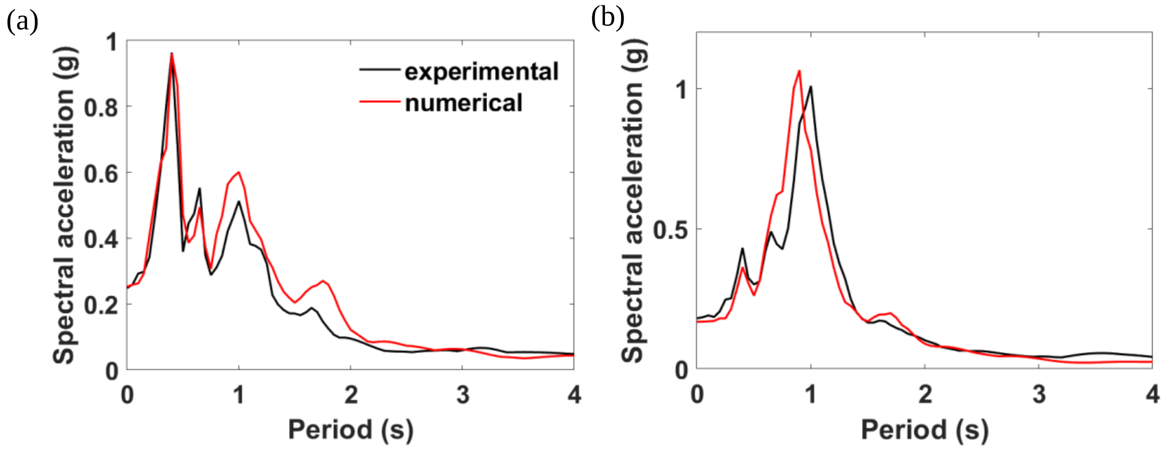

Fig. 7. Acceleration response spectra comparing the measured responses of (a) free-field motion at ground surface and (b) pile-head motion, from the centrifuge test of [35] with the numerical results.

4. Properties of pier-pile-soil system and ground motions

4.1. FE modelling

A typical pier-pile-group foundation system designed in accordance with the Indian Standard (IS) codes and the relevant Indian Road Congress (IRC) recommendations [36-40]. The foundation consists of a pile group comprising of six piles (2 × 3 pile configuration), each with a diameter (D_{pile}) of 1.2 m and a length of 25 m, embedded in homogeneous sandy soil. The pier and the fixed-head piles are rigidly connected by an RC cap of 1.8 m thick. To minimize overlapping influence zones and stress interactions between adjacent piles, the centre-to-centre spacing of piles is set at three times the pile diameter. The pile cap is assumed to be resting on the ground, positioning the pile-heads at the ground level. The pier has a length of 7.5 m and a diameter (D_{pier}) of 2.1 m. Fig. 8 provides detailed dimensions and configurations of the system. The considered concrete grades are M55 for the pier and M40 for the piles. For both the pier and piles, the longitudinal reinforcement has a yield strength of 500 MPa and a Young's modulus of 200 GPa. The longitudinal reinforcement ratio is 1.38% for the pier and 2% for the piles (for the reference case).

A BNWF-based three-dimensional (3D) FE model of the pier-pile-soil system is developed using OpenSees (Fig. 9) and following the methodology outlined in Section 2. The pile-cap is modelled using elastic beam-column elements with very high rigidity. Mass of the superstructure is applied at the pile head, while the pile-cap mass is assigned at the centre of the pile cap. Subsequently, the pier-pile-soil system considered in this study exhibits greater stiffness in longitudinal direction and comparatively weaker resistance in the transverse direction. Therefore, the analysis is conducted in the transverse direction, with loads applied perpendicular to the longitudinal axis of the bridge.

4.2. Adopted ground motions

This study uses a suite of 12 Ground Motions (GMs) from the Pacific Earthquake Engineering Research Center (PEER) [41] ground motion database, selected based on the magnitude (M), source-to-site distance (R), and Peak Horizontal Acceleration (PHA) criteria [2]. Two sets of motions, 6 low-to-moderate and 6 medium-to-very strong-earthquakes have been considered:

- Sub-set 1 (low-to-moderate, far-field motions): $0 < \text{PHA} \leq 0.4\ g$, M > 6, R< 12 km,
- Sub-set 2 (medium to very strong, near-field motions): $0.4\ g < \text{PHA} \leq 1.3\ g$, M > 6, R > 12 km.

As stated by [2], this procedure of ground motion selection is suitable for developing fragility curves for a specific bridge class under any seismic environment. However, when assessing the fragility of a particular bridge at a specific site, a site-specific probabilistic seismic hazard assessment is required. Table 1 lists the information on the selected ground motions, including the record sequence number (RSN) in the PEER ground motion database.

The present study adopts the term PHA instead of Peak Ground Acceleration (PGA). The difference lies in the fact that PGA typically refers to the maximum acceleration in the time

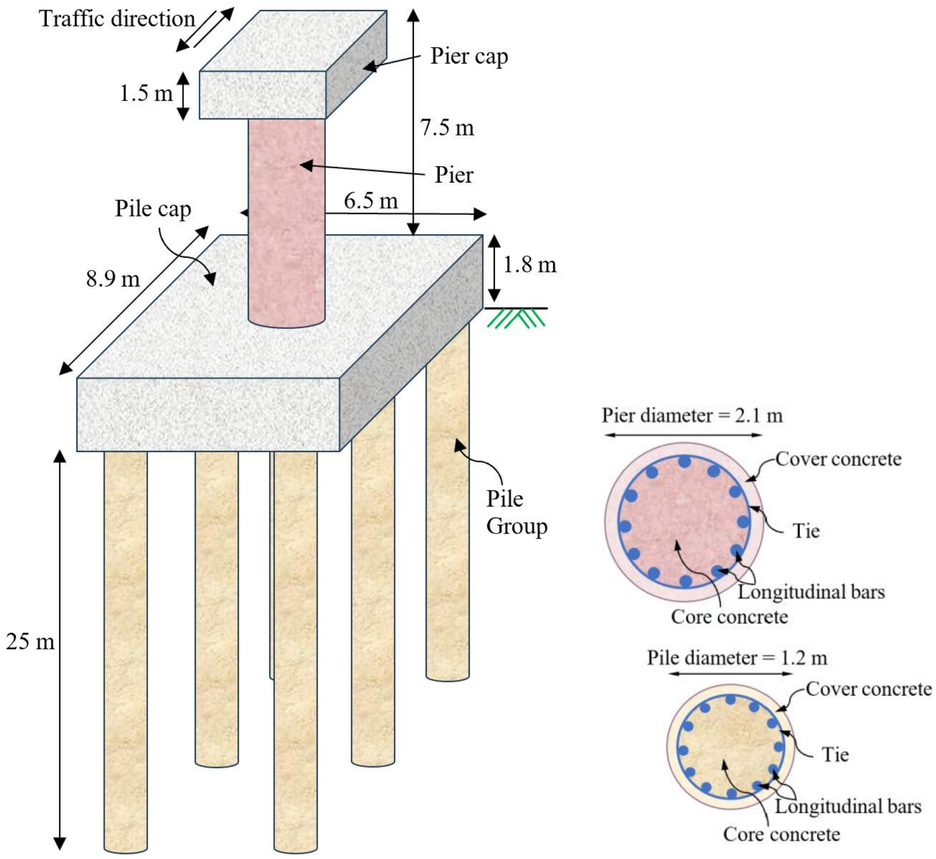

Fig. 8. Schematic illustration of the pier-pile-group foundation system (Reference case).

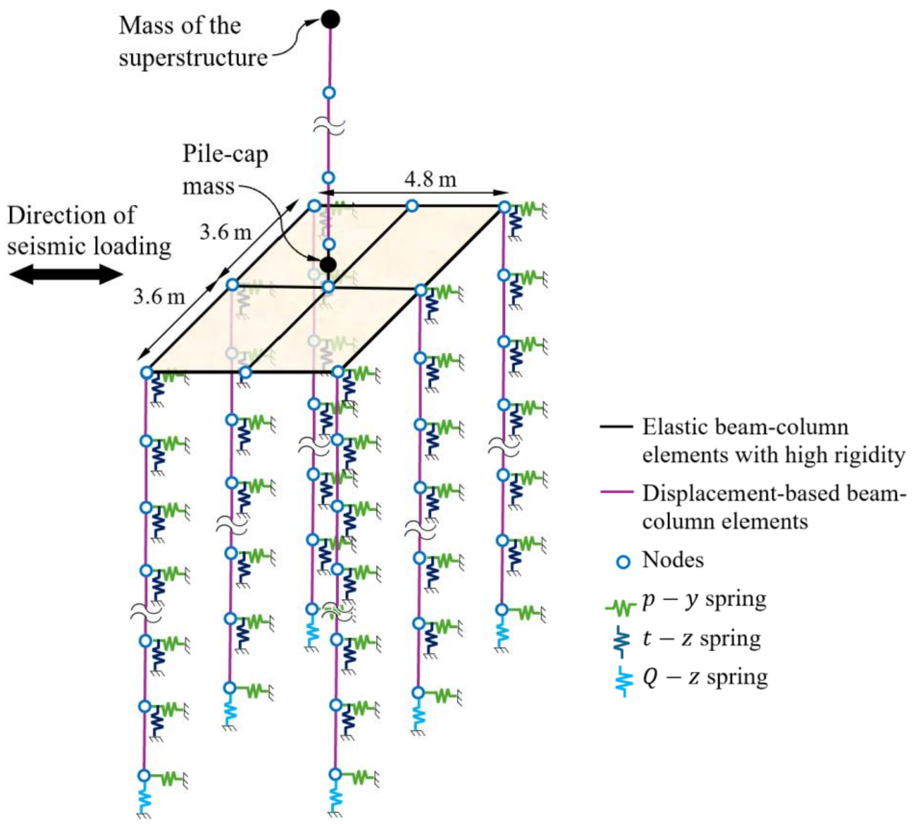

Fig. 9. Schematic illustration of the BNWF-based FE model of the pier-pile-soil system.

history of a specific earthquake record, which may not necessarily correspond to the peak acceleration experienced at the ground surface. In the context of this study, the ground acceleration values are expected to vary continuously as seismic waves propagate from the bedrock level to the ground surface, a phenomenon captured through site response analysis.

The use of PHA provides a consistent term applicable across all levels of the soil-structure system, whether at the bedrock, foundation, or ground surface.

Table 1
Ground motion parameters (unscaled).

Ground Motion ID	RSN	Earthquake	Station	M	R (km)	PHA (g)
1	6901	Darfield, New Zealand	FDCS	7.00	91.59	0.102
2	166	Imperial Valley	Coachella Canal	6.53	50.10	0.116
3	15	Kern County	Taft Lincoln School	7.63	38.89	0.159
4	790	Loma Prieta	Richmond City Hall	6.93	87.87	0.125
5	980	Northridge-01	Huntington Beach	6.69	77.45	0.091
6	578	Taiwan	Smart1 O02	7.30	57.13	0.242
7	1182	Chi-Chi, Taiwan	CHY006	7.62	9.76	0.358
8	160	Imperial Valley-06	Bonds Corner	6.53	2.66	0.598
9	1106	Kobe	KJMA	6.90	0.96	0.834
10	30	Parkfield	Cholame - Shandon Array #5	6.19	9.58	0.443
11	77	San Fernando	Pacoima Dam	6.61	1.81	1.239
12	143	Tabas, Iran	Tabas	7.35	2.05	0.854

4.3. Studied parameters

A parametric investigation is conducted to evaluate the influence of key parameters of piles on the seismic fragility curves and plastic hinge formation of the pier-pile-soil system. A reference case was established first, as previously discussed (designed as per Indian codal provisions) and schematically illustrated in Fig. 8. Maintaining consistent pier parameters, the study considers various pile characteristics, including longitudinal reinforcement ratio (ρ_{l_pile}) and pile diameters (D_{pile}), as well as two different sand types (Loose Sand: LS and Dense Sand: DS). The sand is assumed to be dry and uniform along the entire pile length.

Table 2 presents a summary of the parameters and their values for the six cases considered. Three cases for one studied parameter are sufficient to capture its impact effectively [42]. Cases C01 to C05 are established by changing one parameter at a time from the reference case [17].

The longitudinal reinforcement ratio ranges from 0.4% to 2% (0.4% being the minimum as recommended by [37, 40]), while pile diameter varies from 0.8 m to 1.2 m, covering a typical range encountered in engineering practice.

Table 2
Parametric values for the considered cases in the present study.

Case	ρ_{l_pile} (%)	D_{pile} (m)	Sand type
C00 (reference)	**2**	**1.2**	**LS**
C01	2	1.2	**DS**
C02	2	**1**	LS
C03	2	**0.8**	LS
C04	**1**	1.2	LS
C05	**0.4**	1.2	LS

For the site response analyses, soil columns with both loose sand and dense sand profiles are excited at the base with a suite of 12 ground motions (Table 1), scaled to different PHAs ranging from 0.1g to 1g (scaling of ground motion is discussed in Section 5.1.1). The basic properties of these soils are listed in Table 3. The site response analysis generates free-field DTHs at various depths within the soil column. In addition to providing the DTHs, the analysis also accounts for the influence of local site conditions.

Table 3
Basic soil properties for site response analysis.

Soil Parameters	Loose Sand	Dense Sand
Mass density (kg/m^3)	1700	2100
Reference shear modulus (kPa)*	5.5×10^4	1.3×10^5
Reference bulk modulus (kPa)*	1.5×10^5	3.9×10^5
Friction angle, φ (°)	29	40
Peak shear strain*	0.1	0.1

* at reference pressure, p'_r = 80 kPa

5. Damage analysis

5.1. Fragility assessment methodology

Vulnerability of any system can be effectively illustrated through fragility analysis, a technique that utilizes fragility functions to establish a probabilistic characterization of structural performance in relation to specific limit states. This method correlates seismic demand and structural capacity to assess vulnerability. A fragility function represents the probability of reaching or exceeding a specific damage state corresponding to a given ground motion intensity measure (IM). Fragility curves are commonly represented using a lognormal cumulative distribution function, as outlined below:

$$P[D \geq C|IM] = \Phi\left(\frac{ln\left({S_D}/{S_C}\right)}{\sqrt{\beta_{tot}^2}}\right) \quad (1)$$

where D is the demand; C is the capacity; Φ is the standard normal distribution function; S_D and S_C are median values of the demand and capacity, respectively; β_{tot} is the total uncertainty value calculated as $\beta_{tot} = \sqrt{\beta_C^2 + \beta_D^2 + \beta_{LS}^2}$, where, β_C is the uncertainty in capacity; β_D is the uncertainty in demand; β_{LS} is the uncertainty in limit state definition (for capacity thresholds).

In a past study, the uncertainties in capacity, demand, and damage state definition were estimated through a combination of advanced nonlinear analyses for detailed assessments and simplified elastic models for practical applications to large bridge stocks, employing reduced sampling techniques to balance computational efficiency with reliability in generating bridge-specific fragility curves [43]. Given that generating these uncertainty values requires an extensive number of samples and analyses, substantially increasing computational costs, this study adopts the β values provided by [43].

5.1.1 Seismic demand

Although various static analysis methods are prevalent for assessing seismic demand, nonlinear time history analysis remains the most robust and reliable approach for demand estimation. In the present study, Incremental Dynamic Analysis (IDA) is employed to evaluate the seismic demand of the pier-pile-soil system. To carry out IDAs, selected ground motion records (Table 1) are first scaled to different levels of PHA, ranging from 0.1*g* to 1*g*, with PHA serving as the chosen IM. The scaled GM records are applied at the base of the soil columns to perform site response analysis, accounting for local soil conditions. The resulting DTHs from the site response analysis are then applied to the pile-group foundation.

The displacement at the pier head is considered as the Engineering Demand Parameter (EDP) for each analysis. The maximum lateral displacement at the pier-head corresponding to each scaled earthquake intensity is plotted to construct an IDA curve for each GM record. Subsequently, the median EDP value is calculated for each IM across all GM records. This process is repeated for all cases listed in Table 2. Fig. 10 presents the IDA curves of the RC bridge pier for the reference case (C00) under 12 GMs.

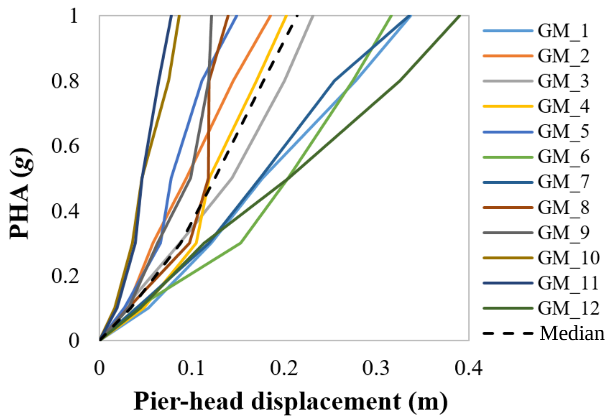

Fig. 10. IDA curves of the RC bridge pier for the reference case.

5.1.2 *Definition of damage limit states*

In seismic design, bridge piers are allowed to undergo inelastic deformation, leading to large displacements and significant damage in plastic hinge zones. Damage in RC bridge piers initiates with cracks, progressing to yielding of longitudinal reinforcement, concrete spalling, core crushing and reinforcement buckling [44]. This damage progression is directly correlated to the tensile and compressive strains in steel reinforcement and concrete. Damage states are often categorized qualitatively as slight, moderate, extensive, and complete [45]. Quantitative limits, based on strain in steel and concrete, are defined to align with qualitative damage states. The five Damage Limit States (DLS) considered in this study for assessing bridge pier performance are listed in Table 4.

Table 4
Considered damage limit states of bridge pier.

Damage Limit States	Damage description	Strain Limit States
DLS1: slight	First cracking of concrete	$\varepsilon_c = \varepsilon_{ctu}$
DLS2: minor	Yielding of longitudinal bar	$\varepsilon_s = \varepsilon_{sy}$
DLS3: moderate	Spalling of cover concrete	$\varepsilon_c = \varepsilon_{cu}$
DLS4: extensive	Crushing of core concrete	$\varepsilon_{cc} = \varepsilon_{ccu}$
DLS5: complete	Buckling of longitudinal bars	$\varepsilon_s = \varepsilon_{s,bb}$

Here, ε_c represents the cover concrete strain, ε_{ctu} denotes tensile strain of cover concrete at the initiation of cracking, ε_s is the longitudinal bar strain, ε_{sy} is the strain in the longitudinal bar at the initiation of yielding, ε_{cu} corresponds to the strain in cover concrete at the initiation of spalling, ε_{cc} corresponds to the core concrete strain and ε_{ccu} corresponds to the strain in core concrete at the initiation of crushing. The subscripts u, y and bb indicate ultimate, yield and bar buckling, respectively. The first four strain limit states are directly obtained from the constitutive material models corresponding to concrete and steel fibres. However, the strain in the longitudinal bar at the initiation of buckling, $\varepsilon_{s,bb}$, cannot be derived directly and is estimated using the equation proposed by [46], and given by,

$$\varepsilon_{s,bb} = 0.3 + 700\rho_s \frac{f_{yh}}{E_s} - 0.1 \frac{P}{f'_{ce} A_g} \tag{2}$$

where, E_s = modulus of elasticity of transverse reinforcement; P = column axial load; f'_{ce} = expected compressive strength of concrete material; and A_g = gross cross-section area of the column.

5.1.3 Estimation of lateral shear capacity

Nonlinear static pushover analyses are performed to determine the lateral shear capacity of the bridge pier for all the six cases under consideration. The analysis employs a displacement-controlled approach with the target lateral displacement set to 0.5 m to ensure that the full nonlinear response of the pier–pile system is captured, including yielding, plastic hinge development, and near collapse level. This level of displacement corresponds to high drift ratios (typically 5–10% for common pier heights), consistent with collapse-level performance objectives in performance-based seismic assessments [44]. For each limit state threshold, the pier-head displacement of the pier-pile-soil system is recorded, corresponding to the monitored strain at the critical section of the pier. Table 5 lists the values of pier-head displacements for all the cases. It can be observed that the pier-head displacement increases with reduction in the pile diameter and the longitudinal reinforcement ratio in the piles, for each limit state. This occurs because the pier–pile-soil system becomes more flexible with reduced foundation stiffness, leading to increased deformation under lateral loading.

The increase of pier-top displacements corresponding to the decrease in pile diameter and longitudinal reinforcement ratio indicates that the concrete and steel strains at the critical section of the pier reach their respective damage thresholds at larger global deformations. This trend highlights the influence of foundation flexibility on the displacement capacity of the system. As the stiffness of the pile foundation decreases, the pier experiences higher lateral displacement before reaching the same strain limits, effectively shifting the damage limit states to higher displacement values.

This behaviour suggests that a more flexible foundation system delays the onset of damage in terms of pier-top displacement, although the actual material strains in the pier section may be similar across different configurations. These observations form the basis for defining strain-based damage limit states used in fragility assessment, ensuring that both global system behaviour and local damage mechanisms are appropriately captured.

Table 5
Pier-head displacements from pushover analyses.

Limit States	Pier-head displacements (m)					
	LS					**DS**
	Decreasing D_{pile}			Decreasing ρ_{l_pile}		
	C03	C02	C00 (reference case)	C04	C05	C01
DLS1	0.0133	0.0068	0.0077	0.0082	0.0086	0.0042
DLS2	0.0748	0.0482	0.0470	0.0512	0.0585	0.0301
DLS3	0.1260	0.0931	0.0911	0.0964	0.1073	0.0716
DLS4	0.3715	0.3312	0.3286	0.3348	0.3495	0.3067
DLS5	0.4984	0.4468	0.4563	0.4626	0.4764	0.4207

The procedure of fragility assesment of the pier-pile-soil system adopted in the study is summarised through the flowchart presented in Fig. 11.

5.2. Plastic hinge formation

The IDAs carried out in this study on the pier-pile-group foundation system are used to examine the local damage of the pier and piles in terms of plastic hinge formations. Plastic hinges typically develop at locations experiencing maximum bending moments within structural elements. For piers, the primary plastic hinge zone is usually concentrated at the base, near the pier-pile cap junction. In case of piles, the first potential plastic hinge is expected to form close to the pile head, while a second plastic hinge zone may develop at some location along the pile depth, depending on the magnitude of the bending moment. The plastic hinge length of the pier is denoted as L_{p_pier}. For piles, the first and second plastic hinge lengths are denoted as L_{p1} and L_{p2}, respectively (Fig. 12).

The distributed plasticity modelling approach adopted in this study for both pier and piles, enables the formation of plastic hinges at any location by allowing plasticity to spread along the member length. When the bending moment at a cross-section reaches the yield moment (M_y), a plastic hinge is assumed to be formed along with the attainment of yield curvature (κ_y) at that section. This concept has been widely used to determine the plastic hinge lengths (L_p) of structural members such as piles and piers [12, 47, 48].

Plastic hinge lengths can be obtained either by bending moment distribution or curvature distribution within a structural member. However, strain and curvature profiles provide a more reliable measure of damage in reinforced concrete components. Therefore, to identify plastic hinge regions along piers and piles, maximum curvature profiles are utilized. Using the pushover curves, the yield curvature is determined for all the cases, namely C00 to C05. To illustrate this methodology, the maximum curvature profiles of the pier and a single pile from the pile group are plotted for Case C03 as shown in Figs. 13(a) and 13(b), respectively.

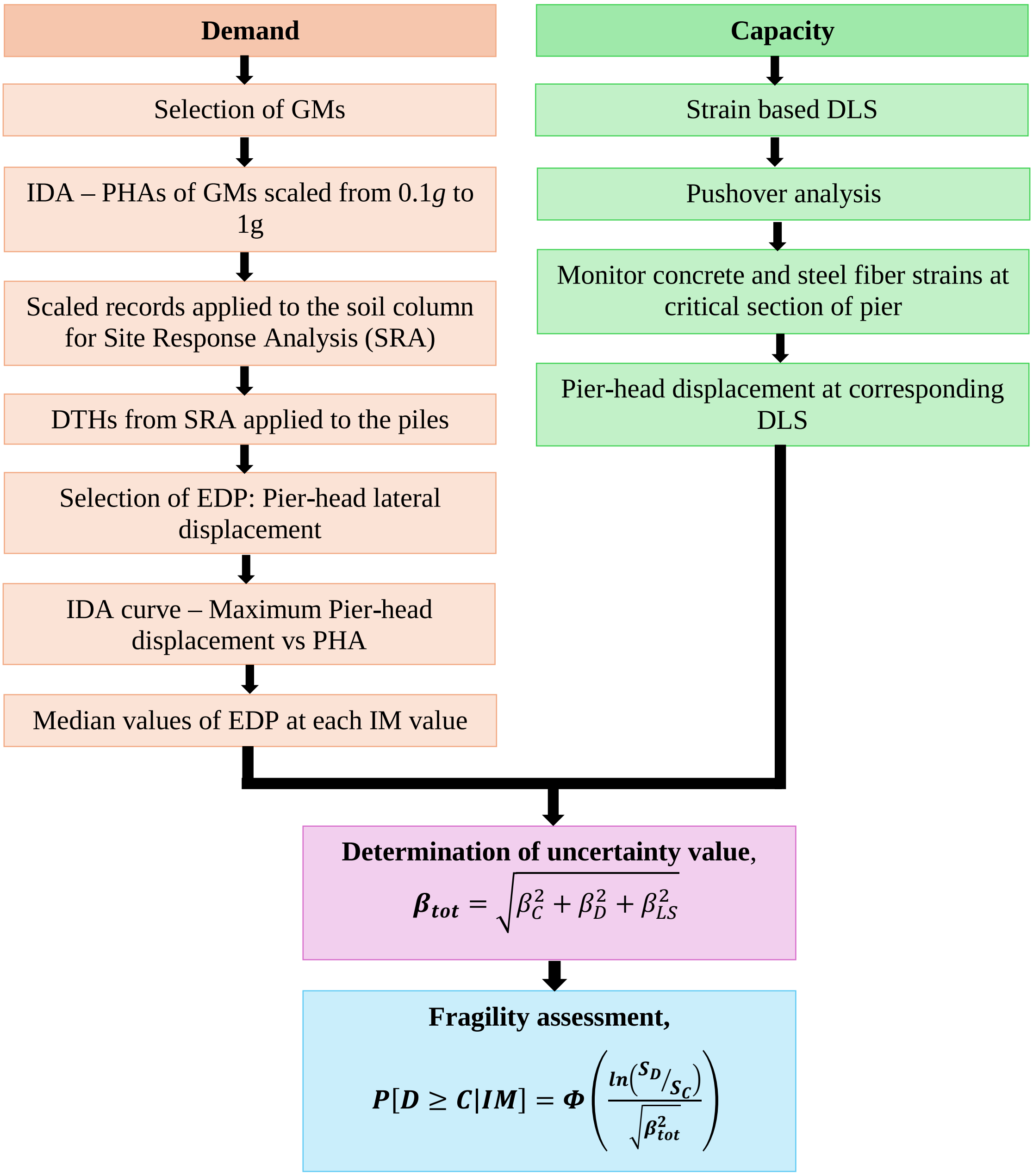

Fig. 11. Flowchart for fragility assesment of the pier–pile-soil system in the present study.

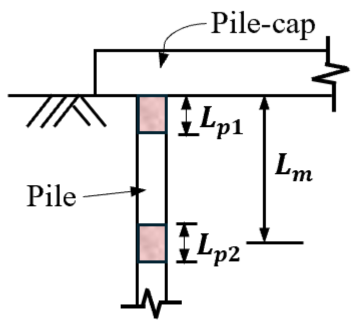

Fig. 12. Schematic representation of plastic hinge zones and location in a pile.

Those profiles are plotted for PHA values ranging from $0.1g$ to $1g$ under Taiwan earthquake. The yield curvatures, indicated by dotted lines on each graph, serve as a threshold for identifying the onset of plastic behaviour.

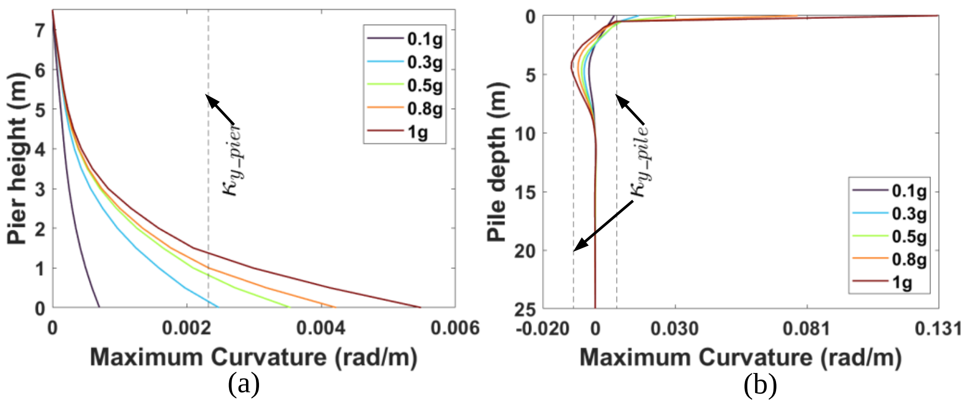

Fig. 13. Maximum curvature profiles of the (a) pier; and (b) pile.

The pier curvature profile reveals distinct regions of high curvature demand, particularly near the base of the pier. For the single pile, the curvature profile shows concentrated regions of high curvature near the pile head and at depths corresponding to the second-highest bending moment along the pile length. Increase in PHA leads to higher extent of the zone with high curvature demand, indicating increased potential plastic hinge lengths. This methodology enables realistic identification of the location and extent of plastic hinge formation in both the pier and the piles.

6. Results

6.1. Local site effects

Nonlinear site response analyses are conducted in both loose and dense sand, considering 12 GMs scaled to the intensity levels of $0.1g$, $0.3g$, $0.5g$, $0.8g$ and $1g$. The variation of the PHA between the bedrock and soil surface for the loose sand and dense sand case is depicted in Figs. 14(a) and 14(b), respectively. These figures demonstrate that higher ground motion intensities result in reduced site amplifications for both soil types, which can be attributed to soil nonlinearity.

Loose sand exhibits a higher amplification factor at lower PHA levels due to its relatively low stiffness. Increase in ground shaking intensity leads to dominance of nonlinear behaviour, and thus a significant reduction in amplification is observed. In contrast, dense sand has a higher stiffness compared to loose sand. Therefore, it exhibits lower amplification at low levels of PHA. The denser packing of particles allows lesser movement and deformation during earthquake shaking, which results in lower amplification. Dense sand shows a more gradual reduction in amplification as PHA increases. This occurs due to their lower nonlinearity, as dense sand tends to show elastic behaviour under increasing stress levels as compared to the loose sand.

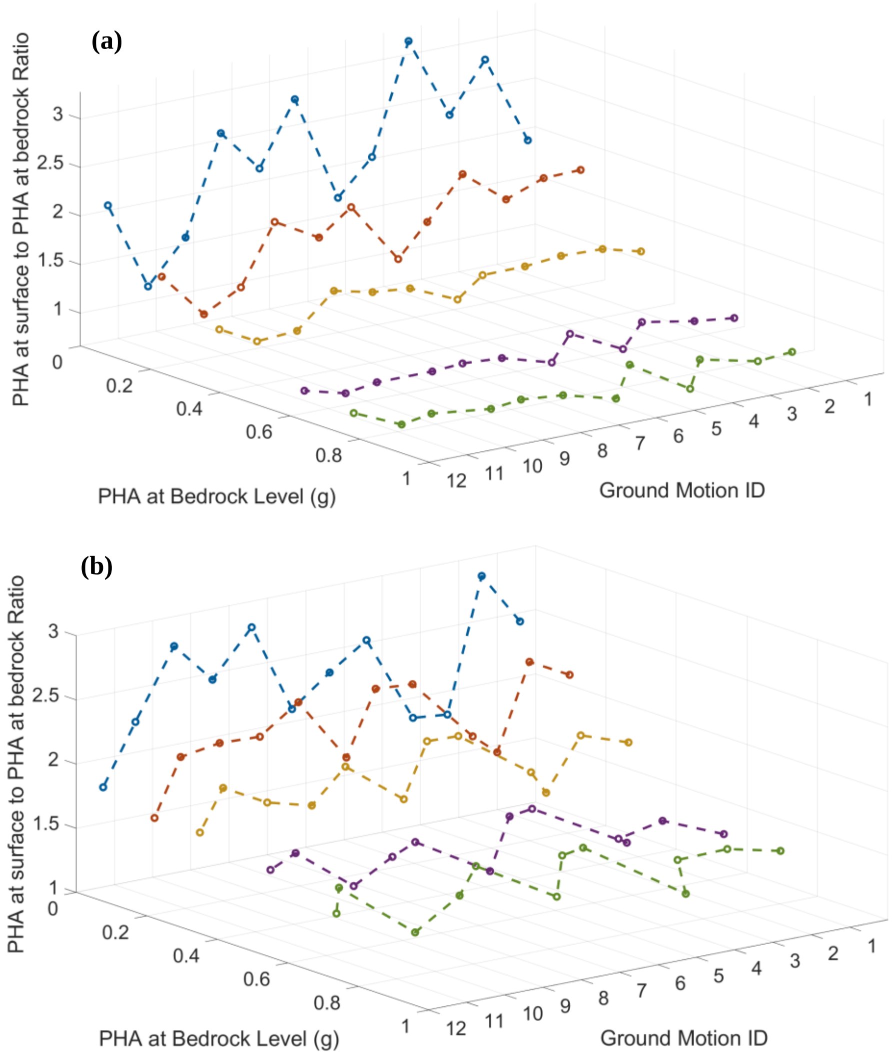

Fig. 14. Variation of PHA value between bedrock and soil surface in (a) Loose sand; (b) Dense sand.

6.2. Fragility assessment

The fragility curves for the RC pier are plotted as shown in Figs. 15, 16 and 17 considering variations in soil type, longitudinal reinforcement ratios of piles, and pile diameters, respectively. The instance of slight damage (DLS1), that is the onset of cover concrete cracking, the damage probability of the pier remains similar across varying parameter values, for example D_{pile} = 1.2 m, 1 m and 0.8 m, under each foundation condition (pile diameter or reinforcement ratio or soil type). This is because the effect of foundation stiffness is more pronounced at higher damage levels when larger curvatures develop, but not as critical at the initial stage of cracking.

6.2.1 Effect of soil type

Fig. 15 presents the probability of damage of the pier as a function of PHA for both loose and dense sand cases. For damage states such as DLS2 and DLS3, corresponding to the yielding of longitudinal reinforcement and the spalling of the cover concrete, respectively, the probability of damage of the pier is higher at lower PHA levels in loose sand condition. This occurs because loose sand exhibits higher amplification at lower PHA compared to dense sand, as dense sand possesses greater stiffness. As PHA increases, the probability of damage for DLS2 and DLS3 increases in dense sand and decreases in loose sand. This is because, at higher PHA levels, loose sand undergoes significant nonlinear behaviour, leading to increased energy dissipation and reduced amplification compared to dense sand. These observations align with the results of the site response analyses.

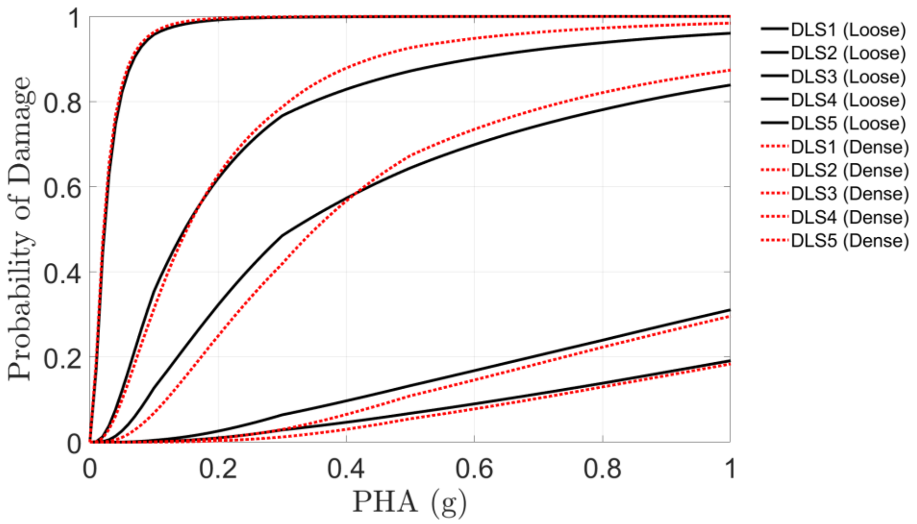

Fig. 15. Fragility curves of the pier for loose and dense sand cases.

However, for the severe damage states, DLS4 and DLS5, corresponding to the crushing of core concrete and buckling of longitudinal steel, the damage probability is higher in loose sand as compared to dense sand, regardless of the ground motion intensity.

6.2.2 Effect of pile longitudinal reinforcement ratio

The probability of damage of the pier across varying longitudinal reinforcement ratios in piles is shown in Fig. 16. As the reinforcement ratio in piles increases, the damage probability corresponding to the yielding of longitudinal reinforcement and the spalling of the cover concrete in the pier also increases. This implies that a stiffer foundation can have detrimental effects on the pier by preventing the piles from yielding, thereby concentrating all nonlinearity in the pier. For DLS4 and DLS5, similar probabilities of core concrete crushing and reinforcement buckling are observed, regardless of the foundation stiffness. This can be attributed to the pier having undergone significant inelastic behaviour, where the remaining resistance is governed more by the material properties (i.e., concrete and steel capacities) than by the effects of foundation flexibility.

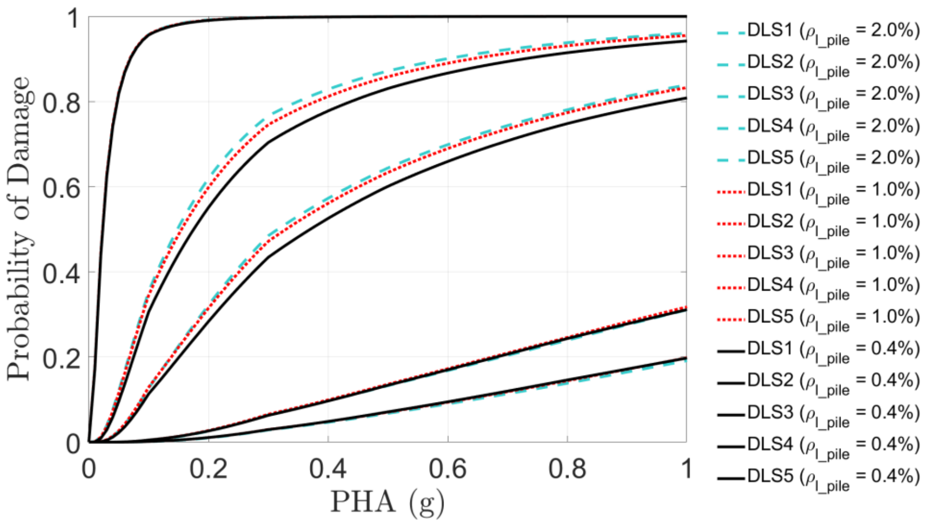

Fig. 16. Fragility curves of the pier with varying longitudinal reinforcement ratios in piles.

6.2.3 Effect of pile diameter

For varying pile diameters, the probability of damage of the pier is shown in Fig. 17. The behaviour of the fragility curves resembles that of the varying soil type case (Fig. 15). For DLS2 and DLS3, a transition phase occurs, shifting the fragility curves for different pile diameters from higher to lower probabilities and vice versa as ground motion intensity increases. This is due to the influence of soil in the pier-pile-soil interaction, as changes in pile diameter tend to change the interacting volume of the surrounding soil. This contrasts with the case of varying reinforcement ratios, where the amount of surrounding soil remains unchanged with the change in reinforcement ratio in the piles.

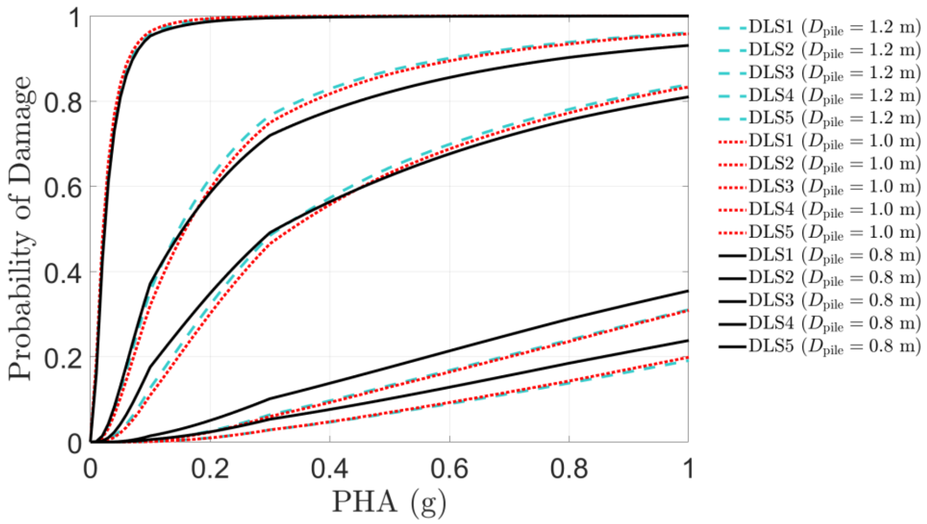

Fig. 17. Fragility curves of the pier considering varying pile diameters.

More specifically, as the pile diameter increases, the effective contact area with the soil also increases. The engagement of a larger extent of the soil, tends to enhance the overall stiffness of the foundation system. At lower ground motion intensities, the increased stiffness reduces amplification, leading to lower damage probabilities. However, at higher intensities the stiffer system may prevent the piles from yielding adequately, thereby concentrating the nonlinearity in the pier and potentially increasing the damage probability.

Conversely, smaller pile diameters result in a reduced volume of interacting soil, which yields a more flexible response. This flexibility can facilitate greater energy dissipation at higher ground motion intensities, thereby reducing damage probabilities for DLS2 and DLS3. For the severe damage states, the damage probability is higher in flexible foundation case (smaller diameter pile) and is lower in stiffer foundation case (larger diameter pile).

6.3. Localised damage progression

Under the applied set of ground motions, the yielded regions along the length of the pier and a single pile in the group (a single pile is selected for representation since all piles in a given case exhibit nearly identical behaviour) are shown in Figs. 18 to 20. In these figures, the plastic hinge zones in the pier are marked in cyan, while the first and second plastic hinge regions in the pile are highlighted in red and blue, respectively. It is to be noted that, for clarity, only half of the pile lengths are depicted, as the other half does not exhibit any plastic hinge formation.

The effect of varying longitudinal reinforcement ratio in pile is examined in relation to the nonlinear behaviour of the pile and pier across five intensities of ground motions, as depicted in Figs. 18(a) and 18(b), respectively. At lower pile reinforcement ratios, the plastic hinges tend to form deeper in the pile, indicating a more flexible response that allows greater energy dissipation through foundation yielding. On the contrary, at higher ρ_{l_pile} values, the plastic hinges shift closer to the pile head, indicating increased pile stiffness, which transfers more inelastic demand to the pier. Fig. 18(b) further shows the increase in plastic hinge length in the pier with the ρ_{l_pile} values. These observations highlight that while increasing the pile reinforcement ratio enhances foundation stiffness and reduces pile yielding, it may also increase inelastic demands on the pier.

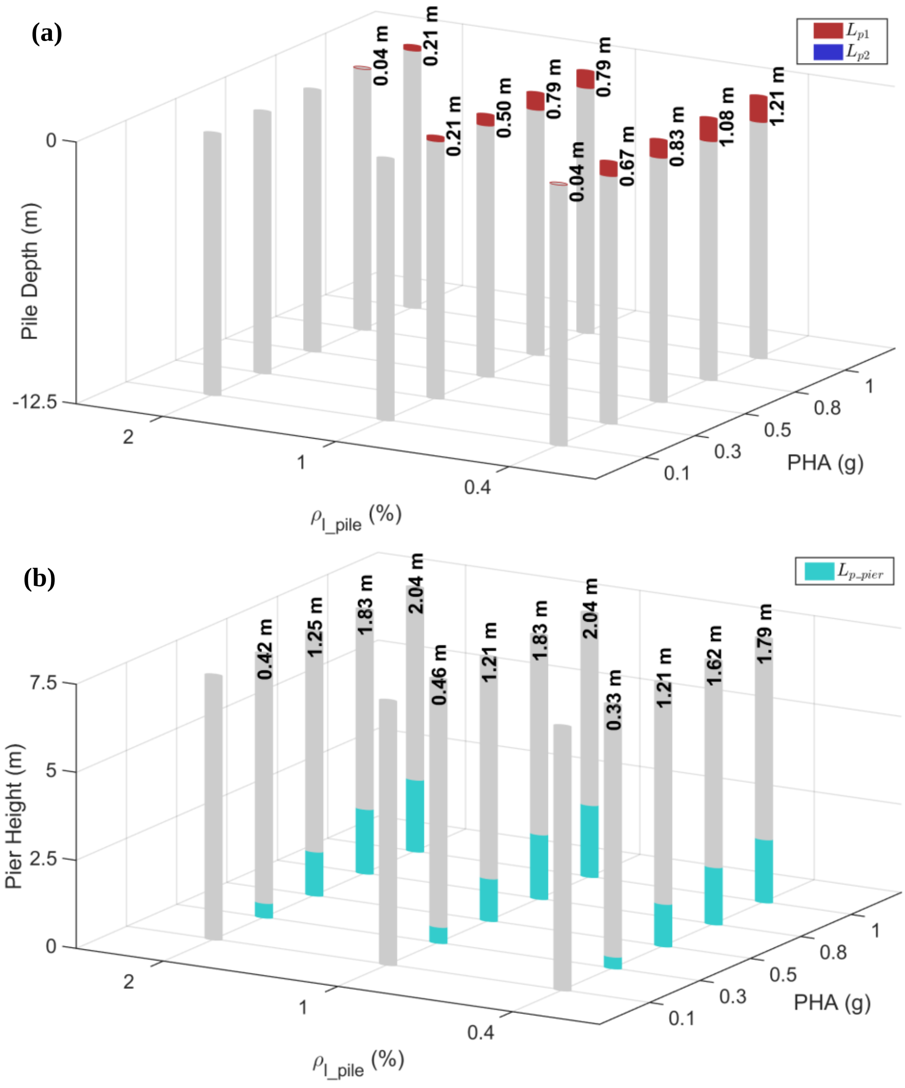

Fig. 18. Plastic hinge zones in (a) a foundation pile and (b) a bridge pier, illustrating the influence of longitudinal reinforcement ratios under varying PHA ranges.

Figs. 19(a) and 19(b) illustrate the influence of variation in pile diameters on plastic hinge formation in the foundation pile and the bridge pier, respectively. For the reference case (Case C00), designed according to Indian Standards, the piles generally do not yield, except under very high-intensity earthquakes, where only slight yielding is observed. In contrast, reduction in pile diameter leads to noticeable yielding in piles, which results in a reduction of the plastic hinge length in the pier. Furthermore, during very high-intensity earthquakes, the second plastic hinge occurs further down the pile length in the 0.8 m diameter pile, which poses a significant concern as retrofitting measures are difficult to implement at such depths.

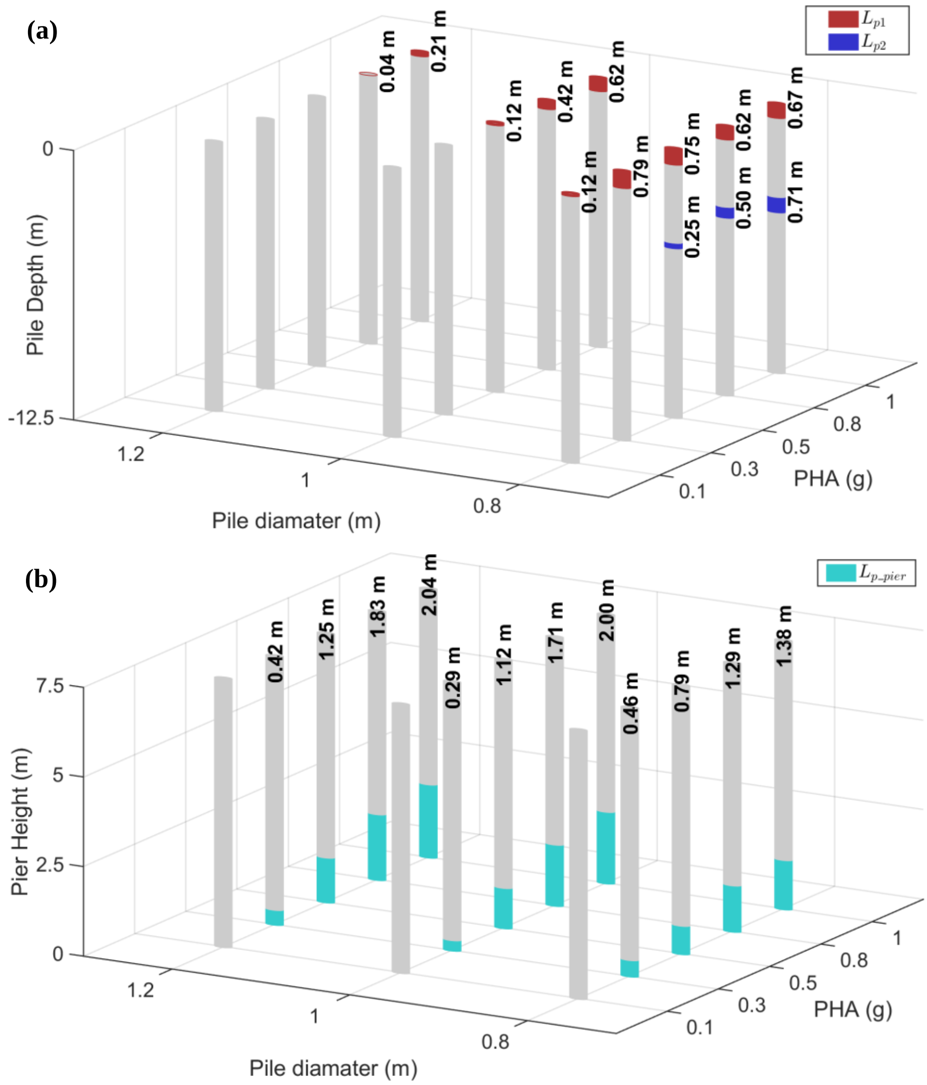

Fig. 19. Plastic hinge zones in (a) a foundation pile and (b) a bridge pier, illustrating the influence of varying pile diameters under varying PHA ranges.

Figs. 20(a) and 20(b) illustrate the inelastic demand on the piles and the pier for loose and dense sand conditions, respectively. The higher stiffness and resistance of the dense sand effectively resist lateral pile displacement. As a result, the majority of the lateral forces are absorbed by the pier rather than the piles causing the pier to experience higher curvatures and plastic hinge formation. The piles, on the other hand, remain in the elastic range because the dense sand provides enough resistance to prevent excessive pile deformation. In the loose sand case, which serves as the reference model (Case C00) and is designed in accordance with current Indian

Standards, the piles exhibit linear elastic behaviour under low to moderate levels of earthquake shaking. This leads to concentration of inelasticity in the pier, which is consistent with the design philosophy that prioritizes inelastic action in structural components that are more accessible for inspection and retrofit.

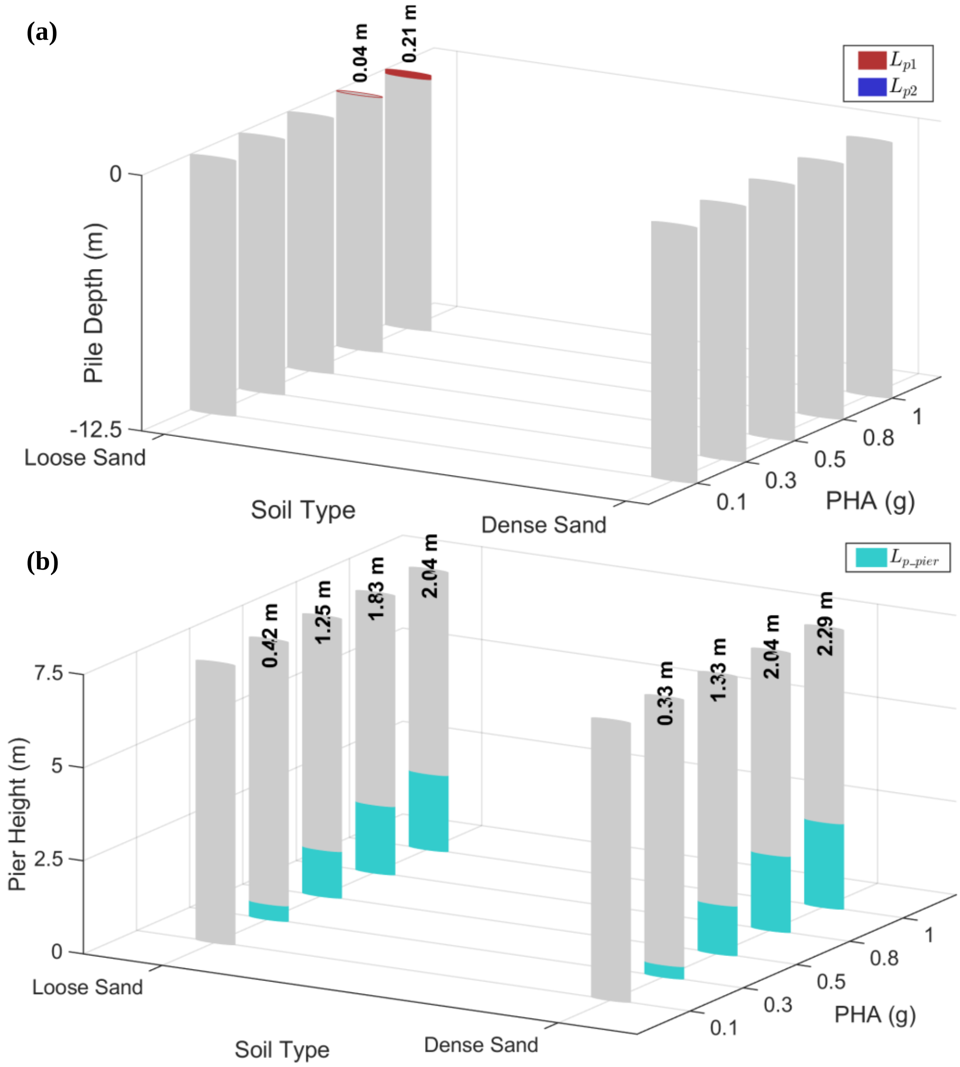

Fig. 20. 3D visualization of plastic hinge zones in (a) a foundation pile and (b) a bridge pier, illustrating the influence of sand type under varying PHA ranges.

7. Conclusions

In this study, the damage probability of an RC bridge pier embedded in sandy soil is evaluated by incorporating the parametric influences of pile and soil properties through a comprehensive pier-pile-soil interaction analysis. The global behaviour of the pier-pile-soil system is assessed through fragility analyses through selection and scaling of GMs to perform IDAs. Site-specific input motions are generated through 1D nonlinear site response analysis based on varying soil types. On selection of the EDP, IDA curves are obtained to estimate seismic demand. For capacity estimation, strain-based damage limit states are defined, followed by pushover analyses of the pier-pile-soil system. Fibre strains are monitored to identify the EDP corresponding to each damage state.

In addition to global behaviour, local damage mechanisms are investigated by observing the development and progression of plastic hinges in both the pier and pile elements. Key parameters such as pile diameter, longitudinal reinforcement ratio in piles, and soil types are varied, as these factors are expected to significantly affect the seismic response of the pier-pile system. The findings of this study, illustrated through fragility curves and three-dimensional visualizations of plastic hinge zones, aim to enhance the understanding of the seismic behaviour of pile-supported bridge piers, providing valuable insights for improving the design strategies and vulnerability assessments of bridge foundations in seismically active regions.

The study demonstrates that the seismic performance of RC bridge pier-pile-soil system is significantly influenced by both pile and soil parameters. A novel methodology is proposed to calculate the plastic hinge lengths and their locations based on the curvature profiles of RC piers and piles under seismic loading conditions. Various foundation configurations are considered, including pile diameters (0.8m, 1m and 1.2m), longitudinal reinforcement ratios (0.4%, 1% and 2%) of piles, and soil types (loose sand and dense sand), to access their influence on the damage probability of the RC pier-pile foundation system. Fragility analysis is used to evaluate the global response of the pier-pile system, while localized damage is analysed by studying the formation of plastic hinges in both piers and piles.

The research findings confirm that the current design practices for RC bridge piers with pile foundations, as dictated by Indian Standards, effectively prevent pile yielding under typical seismic conditions. The piles designed according to these standards do not exhibit significant inelastic behaviour and subsequently formation of plastic hinge zone, even during strong earthquake shaking. This is consistent with the philosophy to keep the foundation elastic to ensure that inelastic deformations and energy dissipation are confined primarily to the pier because repair and retrofitting of damaged piers are comparatively easier than the piles because of convenient access. Furthermore, modifications such as reducing the diameter or the amount of longitudinal reinforcement in the piles lead to pile yielding, which in turn reduces the plastic hinge length in the pier. This adaptation could be beneficial in enhancing the ductility of the overall system by allowing the piles to participate in energy dissipation more actively, thus aligning with the broader goals of seismic design to effectively mobilize seismic energy dissipation without compromising structural integrity.

However, pile diameter and longitudinal reinforcement in pile need to be chosen judiciously to prevent development of plastic hinge zone along the depth of the pile during strong earthquake shaking, due to difficulty in implementing repair and retrofitting measures at that depth.

References

Wang Z, Padgett JE, Dueñas-Osorio L. Influence of soil structure interaction on the fragility of an isolated bridge-soil-foundation system. In 15th World Conference on Earthquake Engineering, Lisbon, Portugal 2012.

Stefanidou SP, Sextos AG, Kotsoglou AN, Lesgidis N, Kappos AJ. Soil-structure interaction effects in analysis of seismic fragility of bridges using an intensity-based ground motion selection procedure. Engineering Structures 2017; 151, 366-380. https://doi.org/10.1016/j.engstruct.2017.08.033

Kwon OS, Elnashai AS. Fragility analysis of a highway over-crossing bridge with consideration of soil–structure interactions. Structure and Infrastructure Engineering 2010; 6(1-2), 159-178. https://doi.org/10.1080/15732470802663870

Guo X, Wu Y, Guo Y. Time-dependent seismic fragility analysis of bridge systems under scour hazard and earthquake loads. Engineering Structures 2016; 121, 52-60. https://doi.org/10.1016/j.engstruct.2016.04.038

Wang X, Ye A, Ji B. Fragility-based sensitivity analysis on the seismic performance of pile-group-supported bridges in liquefiable ground undergoing scour potentials. Engineering Structures 2019; 198, 109427. https://doi.org/10.1016/j.engstruct.2019.109427

Ghimire R, Pradhan P, Gautam D. Multi-hazard fragility analysis of RC bridges for high seismicity and high scouring scenarios. The Journal of Engineering, 2022; (6), 618-628. https://doi.org/10.1049/tje2.12145

Zhang D, Xiong W, Ma X, Cai CS. Fragility evaluation of bridge pile foundation considering scour development under floods. Journal of Bridge Engineering, ASCE 2024; 29(8), 04024052. https://doi.org/10.1061/JBENF2.BEENG-6665

Soltani M, Amirabadi R. Seismic vulnerability assessment of pile-supported wharves using fragility surfaces. Journal of Earthquake Engineering 2022; 26(14), 7140-7155. https://doi.org/10.1080/13632469.2021.1961926

Qiu M, Tian S, Tang L, Cong S, Ling X, Cui J. Development of fragility surfaces for pile-supported structures under mainshock-aftershock sequences. Results in Engineering 2024; 21, 101826. https://doi.org/10.1016/j.rineng.2024.101826

Guettafi N, Yahiaoui D, Abbeche K, Bouzid T. Numerical evaluation of soil-pile-structure interaction effects in nonlinear analysis of seismic fragility curves. Transportation Infrastructure Geotechnology 2022; 1-18. https://doi.org/10.1007/s40515-021-00161-y

Lemsara F, Bouzid T, Yahiaoui D, Mamen B, Saadi M. Seismic Fragility of a Single Pillar-Column Under Near and Far Fault Soil Motion with Consideration of Soil-Pile Interaction. Engineering, Technology & Applied Science Research 2023; 13(1), 9819-9824. https://doi.org/10.48084/etasr.5405

Budek AM, Priestley MJN, Benzoni G. Inelastic seismic response of bridge drilled-shaft RC pile/columns. Journal of Structural Engineering, ASCE 2000; 126(4), 510-517. https://doi.org/10.1061/(ASCE)0733-9445(2000)126:4(510)

Zhang J, Hutchinson TC. Inelastic pile behavior with and without liquefaction effects. Soil Dynamics and Earthquake Engineering 2012; 36, 12-19. https://doi.org/10.1016/j.soildyn.2011.11.007

Goel RK. Evaluation of in-ground plastic-hinge length and depth for piles in marine oil terminals. Earthquake Spectra 2015; 31(4), 2397-2417. https://doi.org/10.1193/071813EQS207M

Heidari M, El Naggar MH. Design guideline for extended pile shaft incorporating nonlinear pile-soil interaction. Ocean Engineering 2022; 243, 109371. https://doi.org/10.1016/j.oceaneng.2021.109371

Zhou L, Barbato M, Ye A. Pile group effect modelling and parametric sensitivity analysis of scoured pile group bridge foundations in sandy soils under lateral loads. Journal of Bridge Engineering, ASCE 2023; 28(8), 04023046. https://doi.org/10.1061/JBENF2.BEENG-5861

Wang J, Wang X, Ye A. Ductile behavior of scoured RC pile-group foundations for bridges in cohesionless soils: parametric incremental dynamic analysis. Journal of Bridge Engineering, ASCE 2023; 28(9), 04023057. https://doi.org/10.1061/JBENF2.BEENG-5942

McKenna F. OpenSees: A framework for earthquake engineering simulation. Computing in Science & Engineering 2011; 13(4):58–66. DOI: 10.1109/MCSE.2011.66

Park R, Priestley MN, Gill WD. Ductility of square-confined concrete columns. Journal of the Structural Division, ASCE 1982; 108(4):929–950. https://doi.org/10.1061/JSDEAG.0005933

Scott BD, Park R, Priestley MJ. Stress-strain behaviour of concrete confined by overlapping hoops at low and high strain rates. American Concrete Institute 1982; vol. 79, no. 1, pp. 13–27. DOI: 10.14359/10875

Menegotto M, Pinto PE. Method of analysis for cyclically loaded RC plane frames including changes in geometry and non-elastic behaviour of elements under combined normal force and bending. In Proceedings of IABSE Symposium on Resistance and

Ultimate Deformability of Structures Acted on by Well Defined Repeated Loads 1973; Vol. 11, pp. 15-22.

Filippou FC, Popov EP, Bertero VV. Effects of bond deterioration on hysteretic behavior of reinforced concrete joints. Report No. UCB/EERC-83/19, Earthquake Engineering Research Center 1983; University of California, Berkeley, USA.

Boulanger RW, Curras CJ, Kutter BL, Wilson DW and Abghari A. Seismic soil-pile-structure interaction experiments and analyses. Journal of Geotechnical and Geoenvironmental Engineering, ASCE 1999; 125(9), pp.750-759. https://doi.org/10.1061/(ASCE)1090-0241(1999)125:9(750)

Yang Z, Elgamal A, Parra E. Computational model for cyclic mobility and associated shear deformation. Journal of Geotechnical and Geoenvironmental Engineering, ASCE 2003; 129(12), 1119–1127. https://doi.org/10.1061/(ASCE)1090-0241(2003)129:12(1119)

American Petroleum Institute (API). Recommended practice for planning, designing, and constructing fixed offshore platforms. API recommended practice 2000; 2A-WSD (RP 2AWSD), 21st edition, API.

Murchison JM, O'Neill MW. Evaluation of $p-y$ relationships in cohesionless soils. Analysis and Design of Pile Foundations, proceedings of a symposium sponsored by the ASCE Geotechnical Engineering Division, ASCE 1984; National Convention, San Francisco, California, October 1-5, pp. 174-191. https://doi.org/10.1016/0148-9062%2886%2991228-3

Kulhawy FH. Drilled shaft foundations. Foundation Engineering Handbook, 2nd Ed., Chapter 14, H.-Y. Fang ed., Van Nostrand Reinhold, New York; 1991.

Mosher RL. Load-transfer criteria for numerical analysis of axially loaded piles in sand. Part 1: Load-transfer criteria. Technical Report K-84-1, Final Report Army Engineer Waterways Experiment Station; 1984.

Meyerhof GG. Bearing capacity and settlement of pile foundations. Journal of the Geotechnical Engineering Division, ASCE 1976; 102(3), 197-228. https://doi.org/10.1061/AJGEB6.0000243

Vijivergiya VN. Load-movement characteristics of piles. In 4th Symposium of Waterway, Port, Coastal and Occean Div., ASCE 1977; Vol. 2, pp. 269-284.

Allotey N, El Naggar MH. Generalized dynamic Winkler model for nonlinear soil–structure interaction analysis. Canadian Geotechnical Journal 2008; 45(4), 560-573. https://doi.org/10.1139/T07-106

Guedes JPSCDM. Seismic behaviour of reinforced concrete bridges: Modelling, numerical analysis and experimental assessment. PhD thesis, University of Porto, Porto, Portugal; 1997.

Pinto AV, Verzeletti G, Magonette G, Pegon P, Negro P, Guedes J. Pseudo-dynamic testing of large-scale R/C bridges in ELSA. In 11th World Conference on Earthquake Engineering 1996; pp. 23-28.

Kashani MM, Lowes LN, Crewe AJ, Alexander NA. Nonlinear fibre element modelling of RC bridge piers considering inelastic buckling of reinforcement. Engineering Structures 2016; 116, 163-177. https://doi.org/10.1016/j.engstruct.2016.02.051

Gohl B. Response of pile foundations to simulated earthquake loading: experimental and analytical results. PhD thesis. University of British Columbia, USA; 1991.

IS 2911-1-2. Design and construction of pile foundations, Part 1: Concrete piles, Section II: Bored Cast in-situ concrete piles, Bureau of Indian Standards (BIS); 2010.

IS 456. Plain and reinforced concrete – Code of practice, Bureau of Indian Standards (BIS); 2000.

IRC 78. Standard Specifications and Code of Practice for Road Bridges, Section VII, Foundations and Substructure, Indian Road Congress; 2014.

IRC 6. Standard Specifications and Code of Practice for Road Bridges. Section II, Loads and Load Combinations, Indian Road Congress; 2017.

IRC 112. Code of practice for concrete road bridges, Indian Road Congress; 2020.

PEER Center, Pacific Earthquake Engineering Research ground motion database, https://ngawest2.berkeley.edu/ (accessed Feb., 2023)

Ahmed BF, Dasgupta K. Seismic limit states for reinforced concrete bridge pile in sand. Structures 2021; Vol. 33, pp. 128-140. https://doi.org/10.1016/j.istruc.2021.04.027

Stefanidou SP, Kappos AJ. Methodology for the development of bridge-specific fragility curves. Earthquake Engineering & Structural Dynamics 2016; 46(1), 73-93. https://doi.org/10.1002/eqe.2774

Lehman D, Moehle J, Mahin S, Calderone A, Henry L. Experimental evaluation of the seismic performance of reinforced concrete bridge columns. Journal of Structural Engineering, ASCE 2004; 130(6), 869-879. https://doi.org/10.1061/(ASCE)0733-9445(2004)130:6(869)

FEMA HAZUS: Multi-hazard loss estimation methodology earthquake model: Technical manual. Washington; 2017.

Goodnight JC, Kowalsky MJ, Nau J.M. Effect of load history on performance limit states of circular bridge columns. Journal of Bridge Engineering, ASCE 2013; 18(12), 1383-1396. https://doi.org/10.1061/(ASCE)BE.1943-5592.0000495

Chai YH. Flexural strength and ductility of extended pile-shafts. I: Analytical model. Journal of structural engineering, ASCE 2002, 128(5), pp.586-594. https://doi.org/10.1061/(ASCE)0733-9445(2002)128:5(586)

Song ST, Chai YH, Hale TH. Analytical model for ductility assessment of fixed-head concrete piles. Journal of Structural Engineering, ASCE 2005, 131(7), pp.1051-1059. https://doi.org/10.1061/(ASCE)0733-9445(2005)131:7(1051)